Electrochemical characterization of Ti3C2T MXene prepared via a molten salt etching route in an acetonitrile-based electrolyte

Liyuan Liu, Encarnacion Raymundo-Piñero, Pierre-Louis Taberna, Patrice Simon

Electrochemical Characterizations of $Ti_3C_2T_x$ MXene Prepared via Molten Salt Etching Route in Acetonitrile-based Electrolyte

Liyuan Liu[1,2], Encarnacion Raymundo-Piñero[2,3], Pierre-Louis Taberna[1,2]*, and Patrice Simon[1,2]*

[1]CIRIMAT, UMR CNRS 5085, Université Paul Sabatier Toulouse III, 118 route de Narbonne, 31062 Toulouse, France

[2]RS2E, Réseau Français sur le Stockage Electrochimique de l'Energie, FR CNRS 3459, 80039 Amiens Cedex, France.

[3]CNRS, CEMHTI UPR3079, Université Orléans, Orléans, France.

*Corresponding author(s) email(s): pierre-louis.taberna@univ-tlse3.fr, patrice.simon@univ-tlse3.fr.

Abstract

2-dimensional metal carbide and nitride materials (MXene) with controlled Cl- and O-surface terminations (MS-$Ti_3C_2T_x$) were prepared from a molten salt etching route and their electrochemical properties were investigated in nitrile-based electrolytes. Results show that the power performance of MS-$Ti_3C_2T_x$ was greatly improved in acetonitrile (ACN) based non-aqueous organic electrolytes, which are conventional electrolytes for electrochemical capacitors. The addition of lithium salt to reach 2 M LiTFSI in ACN results in the increase of the specific capacitance. Moreover, replacing LiTFSI with LiFSI drastically improves the power performance of MXene at a high scan rate (95 mAh g^{-1} at 900C). These results highlight the importance of properly matching the electrolyte composition to the electrode material and shed light on MXenes materials as high-rate electrodes for energy storage applications.

Key words: $Ti_3C_2T_x$ MXene, molten salts approach, acetonitrile, surface termination, Li-ion battery

1. Introduction

MXenes are a diverse class of layered two-dimensional (2D) transition metal carbides or carbonitrides with the general formula of $M_{n+1}X_nT_x$ (n = 1−3), where M represents an early transition metal, X is carbon and/or nitrogen and T_x represents the surface groups originating from the etchant.[1-4] Since their discovery in 2011, MXenes became one of the most promising 2D materials in various fields, especially the world of electrochemical energy-storage applications thanks to their numerous merits such as metal-like electrical conductivity, controllable layer spacing, tunable surface chemistry, and rich chemical composition.[1-7] Over the past 10 years, MXenes were mainly prepared from the etching of MAX phases (where A is an element of the A column of the periodic table) in aqueous solutions containing fluoride ions (HF[6], LiF+HCl[2]), which gave rise to -F and -OH contained surface-functionalized MXenes (HF-MXenes). Many research investigations have revealed that the tuning of the surface functional groups of MXenes would greatly affect their electronic characteristics and electrochemical features.[8-11] As a result, HF-MXenes were reported to show excellent rate capability and high volumetric capacitance in acidic aqueous electrolytes[3], whereas low capacity and poor rate capability were observed in non-aqueous solutions[12]. The nature and content of the MXene surface terminations are highly dependent on the synthetic route and post-synthesis treatment[13], and designing new synthesis routes for MXene is an important challenge in view of tuning their surface groups.

In 2019, a new method based using Lewis acidic molten salt was reported to prepare MXenes[14], which attracted wide attention from researchers due to its great potential to tune the surface chemistry. By playing with the Lewis acid melt composition, this molten salt synthesis route allows for the preparation of MXene terminated with various surface terminations such as Cl, Br and I.[15] This method allows producing new types

of MXene that are difficult or even impossible to be prepared by using previously reported synthesis methods like HF etching. As a result, it further expands the range of MAX phase precursors that can be used and offer interesting opportunities for tuning the surface chemistry and making MS-MXene promising to be used as a high-rate electrode in a non-aqueous system.

It is well known that the electrochemical performance of MXene is highly dependent on the nature of the electrolyte.[16, 17] In 2019, Wang et al. investigated the electrochemical properties of HF-$Ti_3C_2T_x$ as anodes for Li-ion batteries in three different electrolytes, and observed double capacity when moving from nitrile- and sulfoxide- to carbonate-based solvents.[18] In the present paper, the Li-ion intercalation in Cl and O-terminated MS-$Ti_3C_2T_x$ MXene used as negative electrode was studied in nitrile-based electrolytes. The result shows that using acetonitrile-based electrolyte enables higher conductivity, while presenting a low coulombic efficiency due to the electrolyte reduction occurring at low potential and the absence of Solid Electrolyte Interphase formation; however, the coulombic efficiency could be significantly improved by increasing the Li salt concentration. The above results highlight the influence of the surface terminations group/electrolyte composition combination on the electrochemical performance of MXene materials, and pave the way for designing electrodes for a high-power performance application.

2. Experimental

2.1. Preparation of MS-$Ti_3C_2T_x$

Ti_3AlC_2 (11 tech, CAS # 196506-01-1) was used as the MAX phase precursor, $CuCl_2$ (Sigma-Aldrich, CAS # 7447-39-4) was selected as the main etching molten salt while NaCl/KCl was used as the supporting electrolyte. The above chemical raw materials were mixed in a Ti_3AlC_2:$CuCl_2$:NaCl:KCl = 1:3:2:2 molar ratio, and then annealed inside an Ar-protected furnace at 680 °C for 24 h. After cooling down to room temperature, samples were washed with deionized water to remove the excess of molten

salt and further immersed in a 0.1 M APS ($(NH_4)_2S_2O_8$, Sigma-Aldrich, CAS # 7727-54-0) solution for 4 hours to dissolve the residual Cu. In the next step, the above product was washed with a large amount of deionized water to remove the residual APS, followed by drying under vacuum at 80 ℃ for 12 h.

2.2. Physical Characterizations

X-ray diffraction (XRD) data were collected by a D4 X-ray diffractometer (Bruker, Germany) equipped with CuKα radiation (λ = 0.154 nm). The morphology of the MXenes was observed by a Scanning Electron Microscope (SEM) JSM 7100F (JEOL, Japan) with energy-dispersive X-ray spectroscopy (EDX) capabilities. Temperature-programmed desorption (TPD) was performed under an inert atmosphere (Ar, 100ml min^{-1}). The sample (10-20 mg) was placed in a thermo-balance and heat-treated up to 1300 ^oC at a rate of 10 ^oC min^{-1}. The decomposition products (gas evolved) were monitored by online mass spectrometry (Skimmer, Netzsch, Germany).

2.3. Electrochemical measurements

APS-treated MS-$Ti_3C_2T_x$ powder was mixed with a binder and conductive additive to prepare the working electrodes. 80 wt% of MXenes powders 15 wt% of carbon black and 5 wt% of PTFE binder were mixed and then calendared into films. The electrode films were dried in a vacuum oven at 80 ^oC for at least 10 h. Cu disk was used as a current collector with an electrode mass loading controlled at ~ 1.2 mg cm^{-2}. To prepare the counter electrode, YP-50 activated carbon (Kuraray, CAS #1333-86-4) was mixed with 5% polytetrafluoroethylene binder, rolled into free-standing film, and cut into disc-shaped electrodes. Two layers of 260 μm-thick porous borosilicate glass fibers (Whatman GF/B) were used as the separator. A conventional three-electrode setup was assembled inside the glove box (O_2 < 0.1 ppm and H_2O < 0.1 ppm), with APS-treated MS-$Ti_3C_2T_x$ as a working electrode, YP50 active carbon as counter and silver wire as quasi-reference electrodes. All electrochemical characterizations were done at room temperature using a multichannel VMP3 electrochemical working station (Biologic,

S.A.). Electrochemical impedance spectroscopy (EIS) measurements were carried out in a frequency range from 200 kHz down to 10 mHz, at an open circuit potential with an alternating voltage amplitude of 10 mV.

To evaluate the conductivity of the above electrolytes, a conductivity cell with separate double Pt sheet electrodes was purchased from Metrohm. The two Pt electrodes were fully immersed in the above electrolytes inside the glove box and then connected to the Biologic electrochemical working station. Electrochemical impedance spectroscopy (EIS) measurements were performed at 1 kHz to get the resistance of the above electrolytes at room temperature (300 K). The cell conductivity was firstly calibrated to get the cell constant at 300 K using three standard saturated KCl solutions—their ionic conductivities were 10, 98 and 1413 μS cm^{-1}, respectively. Then the conductivity of the solution can be calculated according to the following equation:

$$\sigma = 1/ R_{1kHz} * K_{cell}$$

where σ is the conductivity of the solution (S cm^{-1}), R_{1kH} is the measured resistance of the solution (ohm) at 1 kHz, K_{cell} is the cell constant(cm^{-1}), determined from the measurements carried out with the standard KCl solutions.

3. Results and Discussion

3.1. Material Characterization of $Ti_3C_2T_x$

Figure 1a shows the XRD patterns of the pristine Ti_3AlC_2 MAX phase precursor before (black) and after (green plot) etching by $CuCl_2$, and after washing in APS to remove Cu (blue plot). Compared to pristine Ti_3AlC_2 precursor, most of the diffraction peaks disappeared right after $CuCl_2$ molten salt etching; combined with the shift of intense (002) peak from 9.64° to 7.96°, this evidences the successful etching of the Al layer from Ti_3AlC_2 to prepare the layered Ti_3C_2 with an interlayer distance expanded from 9.20 (MAX) to 11.08 Å (MXene). The sharp peaks located at 43.29°, 50.43° and 74.13°

can be indexed with Cu metal, which disappeared right after further APS washing as a result of the successful removal of Cu. The SEM image (see Figure 1b) shows clearly visible lamellar few-layers accordion-like morphology, which is a traditional morphology of MXene.[15] Energy-dispersive spectroscopy (EDS) measurements of MS-$Ti_3C_2T_x$ (Figure 1c and d) show the presence of small residual weak Al and Cu peaks corresponding to less than 1 at.%, which is consistent with the previous XRD results. EDS semi-quantitative analysis confirms the presence of Cl (16.8 at.%) and O (20.5 at.%), which are highly likely present as surface groups. In addition, the elemental mapping of Ti, Cl and O (Figure 1d) shows a uniform distribution, suggesting that a part of the original halogen termination is replaced with oxygen-containing functional groups during the APS washing.

To identify the different termination species, temperature-programed desorption, coupled with mass spectroscopy measurements (TPD-MS) were performed on APS treated MS-$Ti_3C_2T_x$. In the 25 – 900 °C temperature range, the weight loss associated with the gas evolution of CO_2, CO and H_2O shows that O-containing and Cl groups as well as adsorbed/intercalated water are the main components of the MS-$Ti_3C_2T_x$ MXene surface (see Figure 1e). The H_2O release observed below 400°C, for all the samples, corresponds to surface adsorbed and intercalated water coming from the washing step.[15] The important CO_2 gas release at 100-600 °C is assumed to originate from the oxidation of carbon from Ti_3C_2 by the APS, which further confirms the high amount of oxygen-containing functional groups. The significant release of CO at ~800 ºC evidences the degradation of the MXene material, where the structure is converted into the cubic TiC_y[19] form, while some C reacts with the remaining O-functional group.[20] Quantitative analysis of CO_2, H_2O and CO achieved from TPD-MS measurements shows a total oxygen content of 15.8% (Table S1).

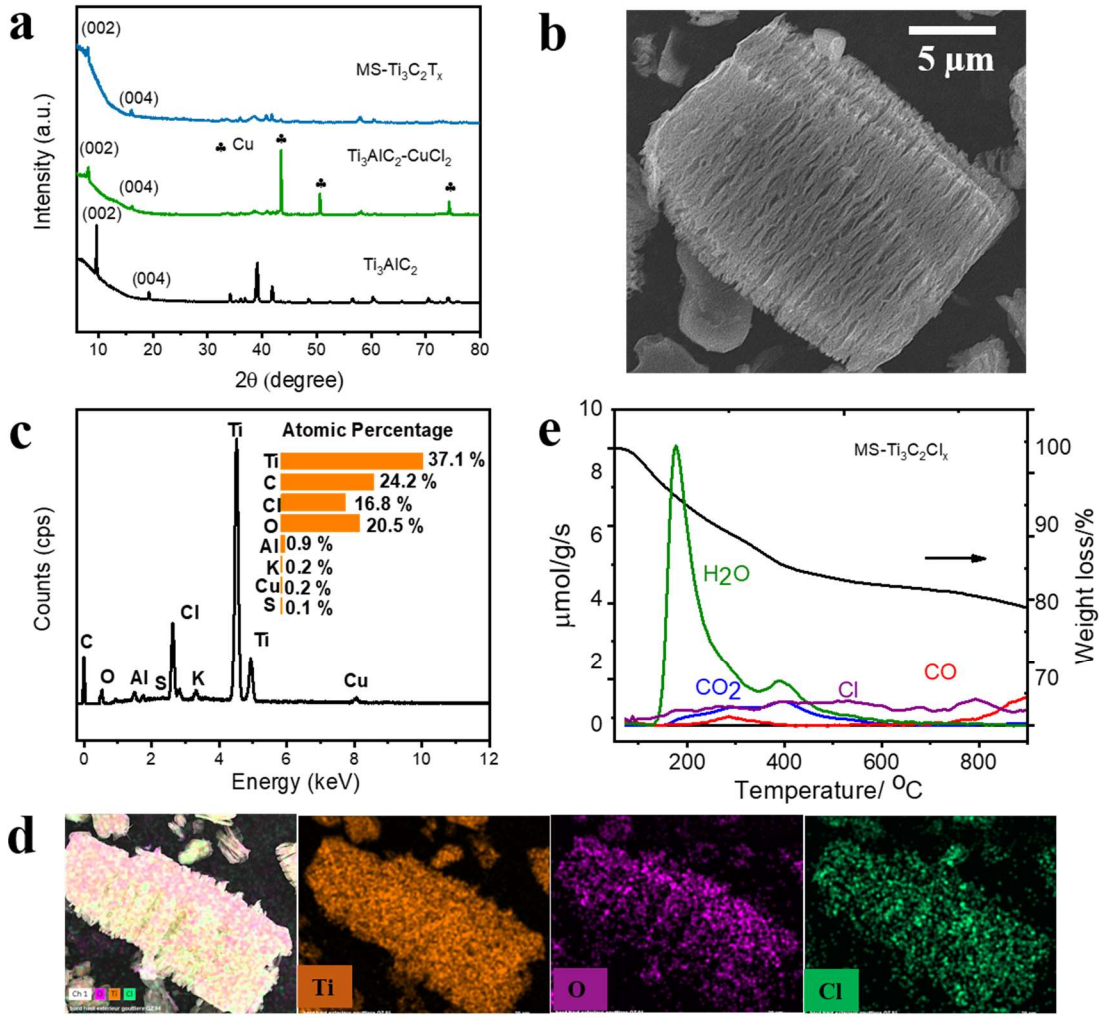

Figure 1. Material characterization of MS-$Ti_3C_2T_x$. (a) XRD patterns of pristine Ti_3AlC_2 before (black line) and after reaction with $CuCl_2$ (green line) followed by washing in 0.1 M $(NH_4)_2S_2O_8$ solution (blue line); (b) SEM images, (c) EDS analysis (d) SEM images and corresponding EDS mapping, and (e) TPD-MS measurements at temperature range up to 900 °C of MS-$Ti_3C_2T_x$.

3.2. Electrochemical Characterizations

3.2.1. Electrochemical Characterizations of LiTFSI in CH_3CN electrolyte

Figure 2a compares the conductivity of four different types of electrolytes with LiFSI (lithium bis(fluorosulfonyl)imide) and LiTFSI (lithium bis(trifluoromethanesulfonyl)imide) salts in nitrile- and carbonate-based solvents. As

expected, LiTFSI and LiFSI in ACN electrolytes achieve a higher conductivity compared to the other types of electrolytes with the same concentration but different solvents (1M LP30: 1M $LiPF_6$ in ethylene carbonate/dimethyl carbonate with 1:1 volume ratio and 1 M LiTFSI in propylene carbonate (PC)). However, the conductivity of LiTFSI in ACN continuously decreases from 37.1 to 2.1 mS cm^{-1} as the concentration increases from 1 M to 4 M, which is similar to LiFSI in ACN (the conductivity decreases from 42.2 to 14.6 mS cm^{-1} from 1 M to 4 M). The maximum potential window of LiTFSI in acetonitrile (ACN) electrolyte was evaluated using a three-electrode cell configuration with small Pt foil as the working electrode, large surface area Pt foil as counter and an Ag wire as a quasi-reference electrode (Figure S1), and tested under Ar atmosphere. As shown in Figure 2b, in both 1 M and 4 M LiTFSI in ACN electrolytes, the high current density measured above 3.0 V vs. Ag and below -3.2 V vs. Ag results in a working potential window of about 6.2 V. However, both the reduction and oxidation current are smaller in 4 M LiTFSI in ACN vs. in 1 M LiTFSI-ACN electrolyte, indicating improved electrolyte stability as the increase of electrolyte concentration. After 5 cycles at 20 mV s^{-1}, as shown in Figure 2c, the color of 1 M LiTFSI in ACN electrolyte turned yellow, while the two platinum disk electrodes became black. On the opposite, the electrolyte of 4 M LiTFSI in ACN (see Figure 2d), remains transparent after testing and the platinum electrodes are still bright. Those visual inspections are very much in line with better electrochemical stability for a higher concentration of LiTFSI, as no visible by-products are formed either in the electrolyte or on the platinum electrodes. Yamada et al. reported the improved electrochemical stability arises from the peculiar structural feature in such superconcentrated solutions with few free ACN solvents that can coordinate the metal cations and the enhanced 3D network further suppresses the diffusion of metal cations into the bulk electrolyte phase [21].

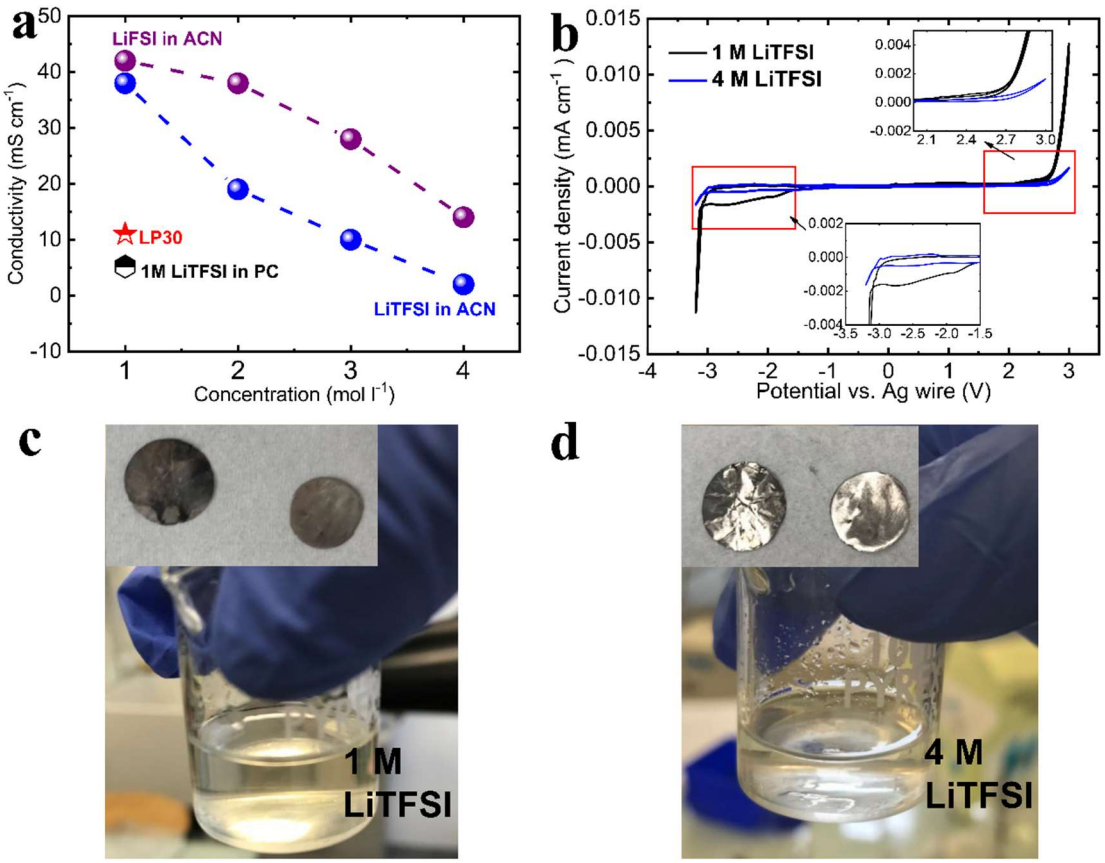

Figure 2: Electrochemical characterization of electrolytes. (a) Ionic conductivity of different types of electrolytes with different concentrations of LiTFSI and LiFSI salts in acetonitrile. The conductivity of 1M LiTFSI in propylene carbonate and LP30 (1M $LiPF_6$ in ethylene carbonate/dimethyl carbonate with 1:1 volume ratio) electrolyte are given for reference. Blank electrolytes test of LiTFSI in ACN electrolyte: (b) CV profile of 1 M and 4 M LiTFSI in ACN scanned at 5 mV s^{-1}; Blank electrolytes and platinum electrodes after scanning at 20 mV s^{-1} for 5 cycles at (c) 1 M LiTFSI in ACN and (d) 4 M LiTFSI in ACN.

Figure 3 shows CVs of MS-$Ti_3C_2T_x$ electrodes tested at LiTFSI in ACN electrolytes with different concentrations of LiTFSI from 1 M to 4 M. The CV area at a large scan rate such as 500 mV s^{-1} turns smaller with the increase of the electrolyte concentration, which can be explained by the decrease in ionic conductivity as shown in Figure 2a. Nevertheless, with 1 M LiTFSI- ACN electrolyte, a low coulombic efficiency of 39% at a low scan rate of 1 mV s^{-1} is obtained due to its lower cathodic stability, compared to 4 M LiTFSI-ACN. With the increase of electrolyte concentration, from 1 M to 4 M,

the coulombic efficiency can be improved from 39% to 88%, at 1 mV s^{-1} (Figure S2). This may be assigned to the lower ionic conductivity; alternatively, the lower amount of free ACN molecules by increasing the concentration of LiTSFI could also play a role here [21, 22]. Interestingly, MS-$Ti_3C_2T_x$ in 2 M LiTFSI electrolyte could achieve the highest capacity of 136 mAh g^{-1} (272 F g^{-1}) compared to other concentrations (see Table 2), while maintaining high power performance of 87 mAh g^{-1} (174 F g^{-1}) with 63% of capacity retention, while it was only 27% and 11% respectively for LP30 and 1 M LiTFSI-PC electrolytes. Despite the slightly decreased ionic conductivity of 2 M LiTFSI in ACN compared to 1 M one, the increased Li-ion concentration suggests more Li^+ can be intercalated inside the MXene layers or absorbed to MXene surface. However, with a further increase of the Li-ion concentrations, the ionic conductivity can be largely increased and results in a lower kinetic behavior and lower capacity.

Figure S3 compares the CVs of MS-$Ti_3C_2T_x$ at 2 M LiTFSI-ACN electrolytes recorded at several potential scan rates with different negative potential cut-offs. As shown in Figure S3a, the electrolyte decomposition starts at a low scan rate below -2.5 V vs Ref. (Ag wire). Thereafter, the negative potential window being limited to -2.3 V vs Ref (Figure 3b), the electrochemical signature is well preserved and the capacity contribution is mainly effective in the -2.3 V to -1.0 V vs. Ag potential range. However, the capacity is largely reduced (65% loss) when the cathodic potential cut-off is limited to -2 V vs. Ag (Figure S3b), indicating that the main capacity contribution comes from the low potential range region, lower than -2 V.

MS-$Ti_3C_2T_x$ has also been tested in LP30 and 1 M LiTFSI-PC electrolytes as shown in Figure S4, using the same cell set-up. Although MS-$Ti_3C_2T_x$ in both electrolytes have similar electrochemical signatures, MS-$Ti_3C_2T_x$ shows a poor rate capability in these two electrolytes, compared to LiTFSI in ACN electrolyte; this expected result is explained by the lower ionic conductivity of PC-based electrolytes vs. ACN-based ones (see Figure 2a, 2 M LiTFSI- ACN: 22.1 mS cm^{-1}, LP30: 11.0 mS cm^{-1} and 1M LiTFSI-PC: 5.2 mS cm^{-1}).

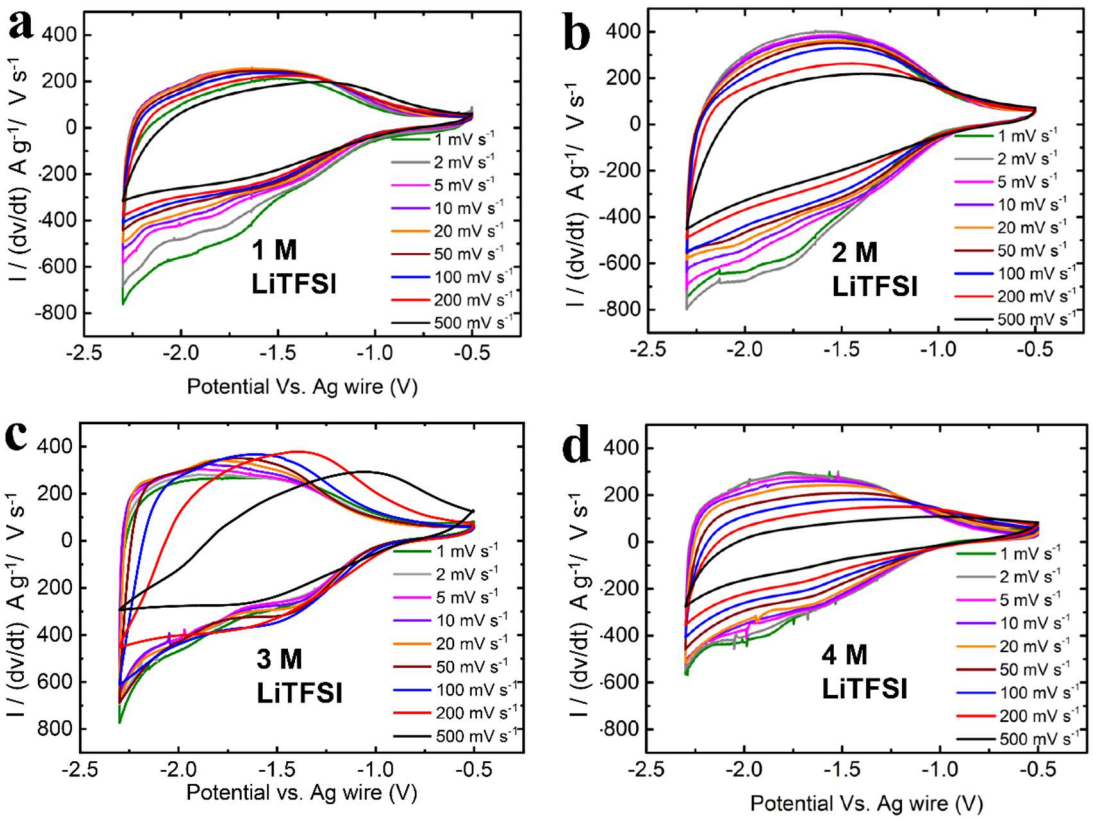

Figure 3: CV curves of MS-$Ti_3C_2T_x$ recorded at various potential scan rates from 1 to 500 mV s^{-1} within a potential window from -2.3 V to -0.5 V vs. Ag at LiTFSI in ACN electrolytes with different concentrations: (a) 1 M, (b) 2 M, (c) 3 M and (d) 4 M.

3.2.2. Electrochemical Characterizations of LiFSI in CH_3CN electrolyte

MS-$Ti_3C_2T_x$ was also tested in 1 M LiFSI in ACN electrolyte due to its high conductivity of 43 mS cm^{-1} (see Figure 2a). Figure 4a shows the cyclic voltammetry profiles of MS-$Ti_3C_2T_x$ collected at potential scan rates from 2 to 500 mV s^{-1}. Remarkably, the CV signature of MS-$Ti_3C_2T_x$ remains capacitive even at high scan rate of 500 mV s^{-1}, giving 110 mAh g^{-1} (220 F g^{-1}) at 2 mV s^{-1} and 95 mAh g^{-1} (190 F g^{-1}) at 500 mV s^{-1}, with a high-capacity retention of 88%. Galvanostatic charge/discharge measurements (Figure 4b) confirm the unique electrochemical signature of the electrode in 1 M LiFSI-ACN non-aqueous electrolyte, with a sloping voltage profile within a potential range of -0.5 – -2.3 V versus Ag wire, as expected from the cyclic voltammetry profiles. However, as shown in Figure S5, the increase of lithium-salt

concentrations to 2 M and 3 M LiFSI in ACN results in a similar capacity of 99 and 101 mAh g^{-1} at 2 mV s^{-1} with lower capacity retention of 65% and 61%, respectively. Figure 4c compares the change of the MS-$Ti_3C_2T_x$ capacitance and capacity with scan rates calculated from cyclic voltammetry at various potential scan rates in 1 M LiFSI in ACN, 2 M LiTFSI in ACN and LP30 electrolytes. The capacitance of MS-$Ti_3C_2T_x$ at 2 M LiTFSI in ACN electrolyte reaches 123 mAh g^{-1} (245 F g^{-1}) at a low scan rate of 5 mV s^{-1}, combined with a coulombic efficiency of 76 % (see Fig. S2). The capacitance remains at 87 mAh g^{-1} (174 F g^{-1}) and the coulombic efficiency goes up to 100% at a high scan rate of 500 mV s^{-1}, corresponding a capacitance retention of 71% as compared to the value of 5 mV s^{-1}, which is much higher than the capacitance retention of 21% measured in LP30. In contrast, despite slightly lower maximum capacity 110 mAh g^{-1} (220 F.g^{-1}) and lower coulombic efficiency (76%), MS-$Ti_3C_2T_x$ in 1 M LiTFSI in ACN electrolyte could achieve the best power capability with 95 mAh g^{-1} (192 F g^{-1}) at 500 mV s^{-1} (equivalent to 900 C) with a capacitance retention of 88%. It also outperforms the electrochemical performance of HF-$Ti_3C_2T_x$ (prepared from conventional LiF/HCl etching method) in LiTFSI - PC electrolyte at similar conditions (see Figure S6) [18], which are the best power performance for MXene electrode reported so far in non-aqueous electrolyte (see Table S3).

Figure 4d shows the Nyquist plots of MS-$Ti_3C_2T_x$ electrode recorded at various bias potentials in 1 M LiFSI -ACN electrolyte. It shows a typical capacitive behavior with a small loop in the high-frequency region associated with a low charge transfer resistance (< 5 ohms, Figure 4d inset), followed by a rapid increase of the imaginary part at low frequencies, which is consistent with a pseudo-capacitive charge-storage mechanism of the MS-$Ti_3C_2T_x$ electrode. This further explains the high-power performance of the MS-$Ti_3C_2T_x$ MXene electrode in 1 M LiTFSI in ACN electrolyte.

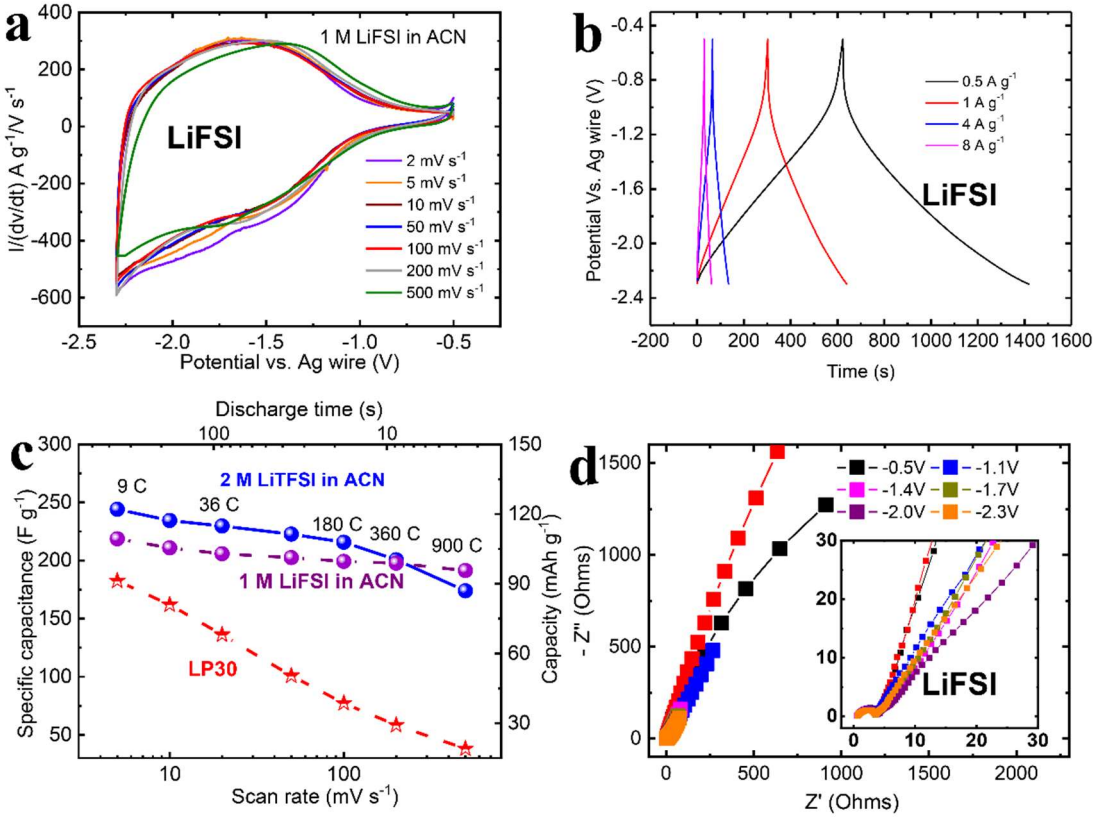

Figure 4: Electrochemical characterizations of MS-$Ti_3C_2T_x$ in 1 M LiFSI in ACN electrolyte. (a) CV curves of MS-$Ti_3C_2T_x$ recorded at various potential scan rates from 2 to 500 mV s^{-1}. (b) Galvanostatic charge/discharge curves at current densities from 0.5 to 8 A g^{-1}. (c) Specific capacitance and capacity evolution with scan rates at different electrolytes. (d) The electrochemical impedance spectroscopy plots recorded at various bias potentials.

4. Conclusion

In this study, the electrochemical behavior of Cl and O-terminated MS-$Ti_3C_2T_x$ was evaluated in different electrolytes prepared from Li salts (LiFSI, LiTFSI) dissolved in nitrile-based solvents. MS-$Ti_3C_2T_x$ shows high power performance in LiTFSI in ACN electrolyte, but with low coulombic efficiency. By increasing the electrolyte concentration from 1 M to 4 M LiTFSI, the coulombic efficiency was drastically improved from 39% to 88% thanks to the enhanced electrochemical stability of the

electrolyte. In contrast, MS-$Ti_3C_2T_x$ materials showed great power ability (87 mAh g^{-1} at 900 C) in 2 M LiTFSI in ACN electrolyte with a decent coulombic efficiency. Moreover, using 1 M LiFSI in ACN electrolyte with higher conductivity, the power performance could be further improved to 95 mAh g^{-1} at 900 C, corresponding to a capacity retention of 88% vs. low-rate discharge. This study shows that properly matching the electrolyte composition to the electrode material offers new opportunities for designing the next generation of high-rate materials for energy storage applications.

Acknowledgements

L.L. was supported by ERC Synergy Grant MoMa-Stor#951513. P.S. and P.L.T. acknowledge the support from Agence Nationale de la Recherche (Labex Store-ex) and ERC Synergy Grant MoMa-Stor #951513.

Reference

[1] B. Anasori, M.R. Lukatskaya, Y. Gogotsi, 2D metal carbides and nitrides (MXenes) for energy storage, Nature Reviews Materials, 2 (2017) 1-17.
[2] M. Ghidiu, M.R. Lukatskaya, M.-Q. Zhao, Y. Gogotsi, M.W. Barsoum, Conductive two-dimensional titanium carbide 'clay'with high volumetric capacitance, Nature, 516 (2014) 78-81.
[3] M.R. Lukatskaya, S. Kota, Z. Lin, M.-Q. Zhao, N. Shpigel, M.D. Levi, J. Halim, P.-L. Taberna, M.W. Barsoum, P. Simon, Ultra-high-rate pseudocapacitive energy storage in two-dimensional transition metal carbides, Nature Energy, 2 (2017) 1-6.
[4] L. Liu, P.-L. Taberna, B. Dunn, P. Simon, Future Directions for Electrochemical Capacitors, ACS Energy Letters, 6 (2021) 4311-4316.
[5] M.R. Lukatskaya, O. Mashtalir, C.E. Ren, Y. Dall'Agnese, P. Rozier, P.L. Taberna, M. Naguib, P. Simon, M.W. Barsoum, Y. Gogotsi, Cation intercalation and high volumetric capacitance of two-dimensional titanium carbide, Science, 341 (2013) 1502-1505.
[6] M. Naguib, M. Kurtoglu, V. Presser, J. Lu, J. Niu, M. Heon, L. Hultman, Y. Gogotsi, M.W. Barsoum, Two-dimensional nanocrystals produced by exfoliation of Ti3AlC2, Advanced materials, 23 (2011) 4248-4253.
[7] L. Liu, M. Orbay, S. Luo, S. Duluard, H. Shao, J. Harmel, P. Rozier, P.-L. Taberna, P. Simon, Exfoliation and Delamination of Ti3C2T x MXene Prepared via Molten Salt Etching Route, ACS nano, 16 (2021) 111-118.
[8] Q. Tang, Z. Zhou, P. Shen, Are MXenes promising anode materials for Li ion batteries? Computational studies on electronic properties and Li storage capability of Ti3C2 and Ti3C2X2 (X= F, OH) monolayer, Journal of the American Chemical Society, 134 (2012) 16909-16916.
[9] Y. Xie, M. Naguib, V.N. Mochalin, M.W. Barsoum, Y. Gogotsi, X. Yu, K.-W. Nam, X.-Q. Yang, A.I. Kolesnikov, P.R. Kent, Role of surface structure on Li-ion energy storage capacity of two-dimensional transition-metal carbides, Journal of the American Chemical Society, 136 (2014) 6385-6394.
[10] G.R. Berdiyorov, K.A. Mahmoud, Effect of surface termination on ion intercalation selectivity of bilayer Ti3C2T2 (T= F, O and OH) MXene, Applied Surface Science, 416 (2017) 725-730.
[11] D. Li, X. Chen, P. Xiang, H. Du, B. Xiao, Chalcogenated-Ti3C2X2 MXene (X= O, S, Se and Te) as a high-performance anode material for Li-ion batteries, Applied Surface Science, 501 (2020) 144221.
[12] R. Cheng, T. Hu, H. Zhang, C. Wang, M. Hu, J. Yang, C. Cui, T. Guang, C. Li, C. Shi, Understanding the lithium storage mechanism of Ti3C2T x MXene, The Journal of Physical Chemistry C, 123 (2018) 1099-1109.
[13] M. Naguib, M.W. Barsoum, Y. Gogotsi, Ten years of progress in the synthesis and development of MXenes, Advanced Materials, 33 (2021) 2103393.
[14] M. Li, J. Lu, K. Luo, Y. Li, K. Chang, K. Chen, J. Zhou, J. Rosen, L. Hultman, P. Eklund, Element replacement approach by reaction with Lewis acidic molten salts to

synthesize nanolaminated MAX phases and MXenes, Journal of the American Chemical Society, 141 (2019) 4730-4737.
[15] Y. Li, H. Shao, Z. Lin, J. Lu, L. Liu, B. Duployer, P.O. Persson, P. Eklund, L. Hultman, M. Li, A general Lewis acidic etching route for preparing MXenes with enhanced electrochemical performance in non-aqueous electrolyte, Nature Materials, 19 (2020) 894-899.
[16] C. Zhong, Y. Deng, W. Hu, J. Qiao, L. Zhang, J. Zhang, A review of electrolyte materials and compositions for electrochemical supercapacitors, Chemical Society Reviews, 44 (2015) 7484-7539.
[17] L. Liu, Z. Lin, J.-Y. Chane-Ching, H. Shao, P.-L. Taberna, P. Simon, 3D rGO aerogel with superior electrochemical performance for K–Ion battery, Energy Storage Materials, 19 (2019) 306-313.
[18] X. Wang, T.S. Mathis, K. Li, Z. Lin, L. Vlcek, T. Torita, N.C. Osti, C. Hatter, P. Urbankowski, A. Sarycheva, Influences from solvents on charge storage in titanium carbide MXenes, Nature Energy, 4 (2019) 241-248.
[19] B.C. Wyatt, S.K. Nemani, K. Desai, H. Kaur, B. Zhang, B. Anasori, High-temperature stability and phase transformations of titanium carbide (Ti3C2T x) MXene, Journal of Physics: Condensed Matter, 33 (2021) 224002.
[20] M. Seredych, C.E. Shuck, D. Pinto, M. Alhabeb, E. Precetti, G. Deysher, B. Anasori, N. Kurra, Y. Gogotsi, High-temperature behavior and surface chemistry of carbide MXenes studied by thermal analysis, Chemistry of Materials, 31 (2019) 3324-3332.
[21] Y. Yamada, K. Furukawa, K. Sodeyama, K. Kikuchi, M. Yaegashi, Y. Tateyama, A. Yamada, Unusual stability of acetonitrile-based superconcentrated electrolytes for fast-charging lithium-ion batteries, Journal of the American Chemical Society, 136 (2014) 5039-5046.
[22] Y. Yamada, J. Wang, S. Ko, E. Watanabe, A. Yamada, Advances and issues in developing salt-concentrated battery electrolytes, Nature Energy, 4 (2019) 269-280.